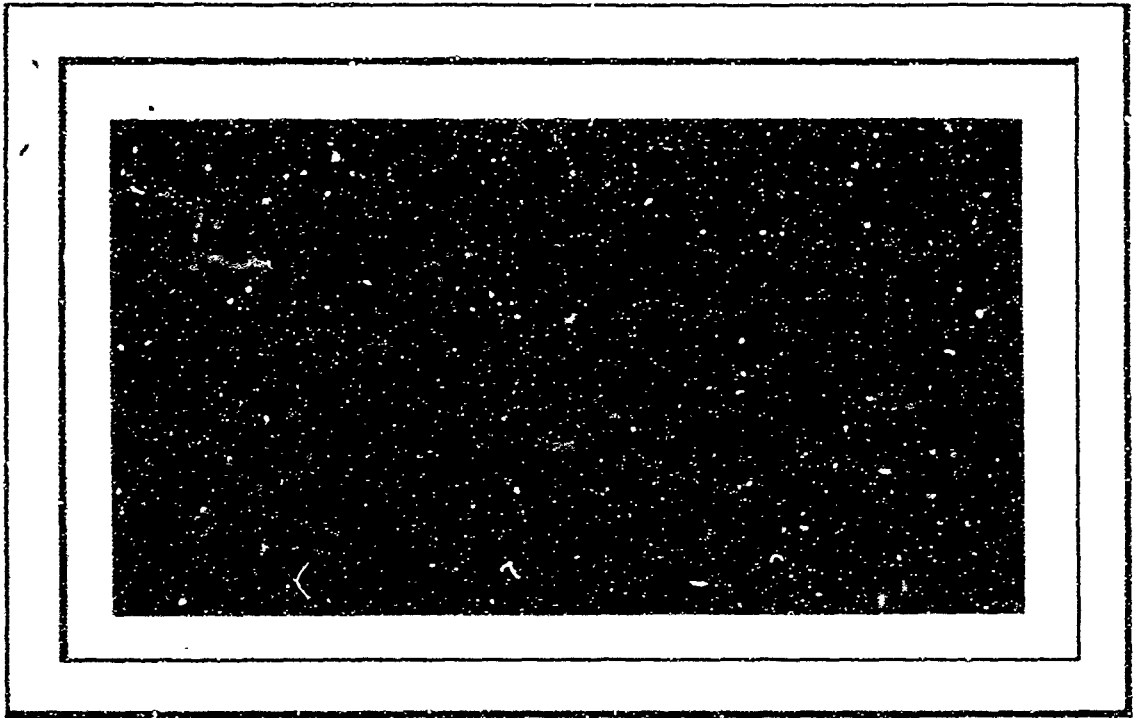


AD 608526



100



COPY	<u>1</u>	OF	<u>1</u>	<u>1</u>
HARD COPY				\$ 3.00
MICROFICHE				\$ 0.75

66p

DDC
 REPRODUCED
 DEC 2 1964
 RESOLVED
 DDC-IRA C

Therm
Advanced
Research, Inc.

100 HUESON CIRCLE • ITHACA, NEW YORK

ARCHIVE COPY

THE DUCTED PROPELLER
IN STATIC AND LOW-SPEED FLIGHT

by

M. D. Greenberg & D. E. Ordway

TAR-TR 6407

October 1964

Submitted to

Air Programs, Office of Naval Research
Washington, D. C.

In partial fulfillment of Contract Nonr-4357(00)

Approved:

A. Ritter

A. Ritter, President

ACKNOWLEDGMENT

The authors wish to acknowledge the help of their colleagues, Messrs. G. R. Hough and A. L. Kaskel. They also wish to acknowledge Elizabeth Cornelius and Susan Tobey for manuscript preparation, and Mr. Y. C. Pao for programming the iterative solution.

Reproduction in whole or in part is permitted for any purpose of the United States Government.

ABSTRACT

A theory is developed for the steady aerodynamic loading on a ducted propeller with finite blade number in static and low-speed flight. The interaction of the higher harmonics with the steady loading is clarified and it is shown that, in a rigorous sense, a high blade-number restriction is required. For a shroud of small camber and zero thickness an analytic solution is obtained, together with simple expressions for shroud thrust and surface pressures, subject to a constant-pitch assumption on the trailing propeller vortices. To be more precise, the pitch hypothesis is dropped and an alternative iterative solution pursued. The final results, however, of an illustrative calculation indicate that the two solutions do not differ significantly. Results of a limited comparison with experiment are quite reasonable.

TABLE OF CONTENTS

INTRODUCTION	1
CHAPTER ONE - FORMULATION	
1.1 Problem Statement	3
1.2 Boundary Conditions and Vortex Model	5
1.3 Evaluation of the Radial Wash	6
1.4 The Resulting Integral Equation	10
CHAPTER TWO - SOLUTION OF THE INTEGRAL EQUATION	
2.1 High Blade-Number Limitation	12
2.2 Determination of Pitch	13
2.3 Solution of the Integral Equation	16
CHAPTER THREE - SHROUD SURFACE PRESSURES AND THRUST	
3.1 Shroud Surface Pressures	19
3.2 Shroud Thrust	22
CHAPTER FOUR - INVESTIGATION OF CONSTANT-PITCH HYPOTHESIS	
4.1 Pitch Iteration	24
4.2 Illustrative Results	27
CHAPTER FIVE - NUMERICAL EXAMPLES	
5.1 Input Data	31
5.2 Results	31
5.3 Comparison with Experiment	33
CONCLUSIONS	37
REFERENCES	38
TABLES	40

PRINCIPAL NOMENCLATURE

c	shroud chord
c_p	shroud surface pressure coefficient; see Eq. (3.1)
c_p^j	net shroud surface pressure coefficient; see Eq. (3.10)
$C_{t,T}$	shroud and propeller thrust coefficients respectively; see Eqs. (3.12), (3.14) and (2.3), (2.4)
g_n	coefficients of Glauert series for steady shroud vortex loading; see Eq. (2.13)
$\underline{i}_{x,r,\theta}$	x, r, θ unit vectors respectively
$[I]$	infinite identity matrix
j	local pitch of trailing propeller vortices
$j_{p,\infty}$	values of j at the propeller plane and infinity respectively
J	$U/\Omega R_p$
N	propeller blade number
p	static pressure
p_∞	static pressure at infinity

[P]	three-dimensional "curvature" matrix
\underline{q}	total fluid velocity vector; see Eq. (1.2)
q_n	coefficients related to propeller-induced camber; see Eq. (2.14)
$Q_{n+\frac{1}{2}}$	Legendre function of second kind and order $(n + \frac{1}{2})$
r_s	shroud radius taken locally
R	shroud radius at propeller plane
R_p	propeller blade radius
[S]	Hough matrix; see Eq. (3.5)
t, T	shroud and propeller thrusts respectively
u, v, w	x, r, θ disturbance velocities respectively; see Eq. (1.2)
U	flight speed
x, r, θ	propeller-fixed coordinates
\bar{x}, \bar{r}	x/R and r/R respectively
γ	bound shroud vortex strength per unit axial length

$\bar{\gamma}$	$\gamma/\Omega R_p$
Γ	bound blade circulation distribution
$\bar{\Gamma}$	$\Gamma/\Omega R_p^2$
δ	flight parameter; $\sigma \equiv J/\sqrt{C_T}$
ϵ	local inclination angle of camber line relative to x-axis; see Fig. 1.1
λ	$c/2R$
$\Lambda_0(\beta, \kappa)$	Heuman lambda function with argument β and modulus κ
μ	R_p/R
ρ	fluid mass density
σ_1, \dots	Legendre function arguments; see Eqs. (1.8), (1.11), (2.11), (4.3), (4.5) and (4.12) respectively
ϕ	Glauert variable; $\bar{x} = -\lambda \cos \phi$
Ω	angular rotational speed of propeller
$()^{(1)}, \dots$	superscript denotes iteration number
$()_0$	subscript 0 denotes zeroth θ -harmonic

- $()_v$ subscript v refers to vortex element
- $()'$ prime denotes differentiation with respect to the indicated argument
- $\{ \}$ infinite column vector
- $\{ \}^T$ transposed vector
- $[\]$ infinite square matrix
- $[\]^{-1}$ inverse matrix

THE DUCTED PROPELLER IN STATIC AND LOW-SPEED FLIGHT

Introduction

In previous studies we have treated the ducted propeller quite extensively for the case of forward flight at zero incidence¹⁻⁴. We now turn our attention to the case of static and low-speed flight, and define the problem as follows: Given the shroud geometry and operating conditions, determine the resulting thrust and time-average surface pressures on the shroud.

In general, study of the static and low-speed problem has been confined to one-dimensional momentum analyses, except for the work of A. R. Kriebel^{5,6} and H. R. Chaplin⁷. Kriebel has obtained an expression for the division of thrust between the shroud and propeller, whereas Chaplin has developed a numerical program directed mainly at computing the slipstream contraction. In both analyses certain restrictions are imposed a priori which limit physical insight into the complicated interactions that arise in static and low-speed operation. Although we will impose essentially the same restrictions except for zero tip clearance, the nature of these interactions will be clarified in the present development. More important,

we will obtain convenient analytic formulas for the shroud thrust and surface pressures.

Analogous to our treatment of the forward-flight condition, we consider first the camber problem, using a classical three-dimensional vortex approach. That is, the shroud and propeller are represented by a distribution of bound ring and line vortices respectively, together with their appropriate trailing vortex systems. The effects of fluid viscosity and compressibility are neglected as well as the presence of a hub, guide vanes and support struts. Once the strength of the bound shroud vortices is determined, the pressures and thrust may be readily computed.

It is anticipated that the contents of this report will be condensed and presented in a tabular format as a simple addition to the procedure of Ref. 4 .

CHAPTER ONE

FORMULATION

1.1 Problem Statement

We consider a ducted propeller in static or steady low-speed flight U at constant rotational propeller speed Ω and zero incidence in an unbounded, inviscid, incompressible fluid otherwise at rest. The term "low-speed" will be made precise later in the analysis.

The shroud is taken to be infinitely thin and of small camber. The N propeller blades are assumed to be infinitely slender, and the hub radius is considered negligible.

In propeller-fixed coordinates x, r, θ the incoming free stream has a uniform translation U in the positive x -direction and a rotational component Ωr in the positive θ -direction, see Fig. 1.1 . The blades are at rest in this system but the duct is rotating about the propeller axis with angular speed Ω . This rotation may, however, be set equal to zero without altering the potential flow since the duct is axisymmetric. The resulting flow field is time-independent but does retain a θ -dependence because of the finite blade number. Taking the propeller blade loading as known, we seek to determine the zeroth θ -harmonic of the shroud loading.

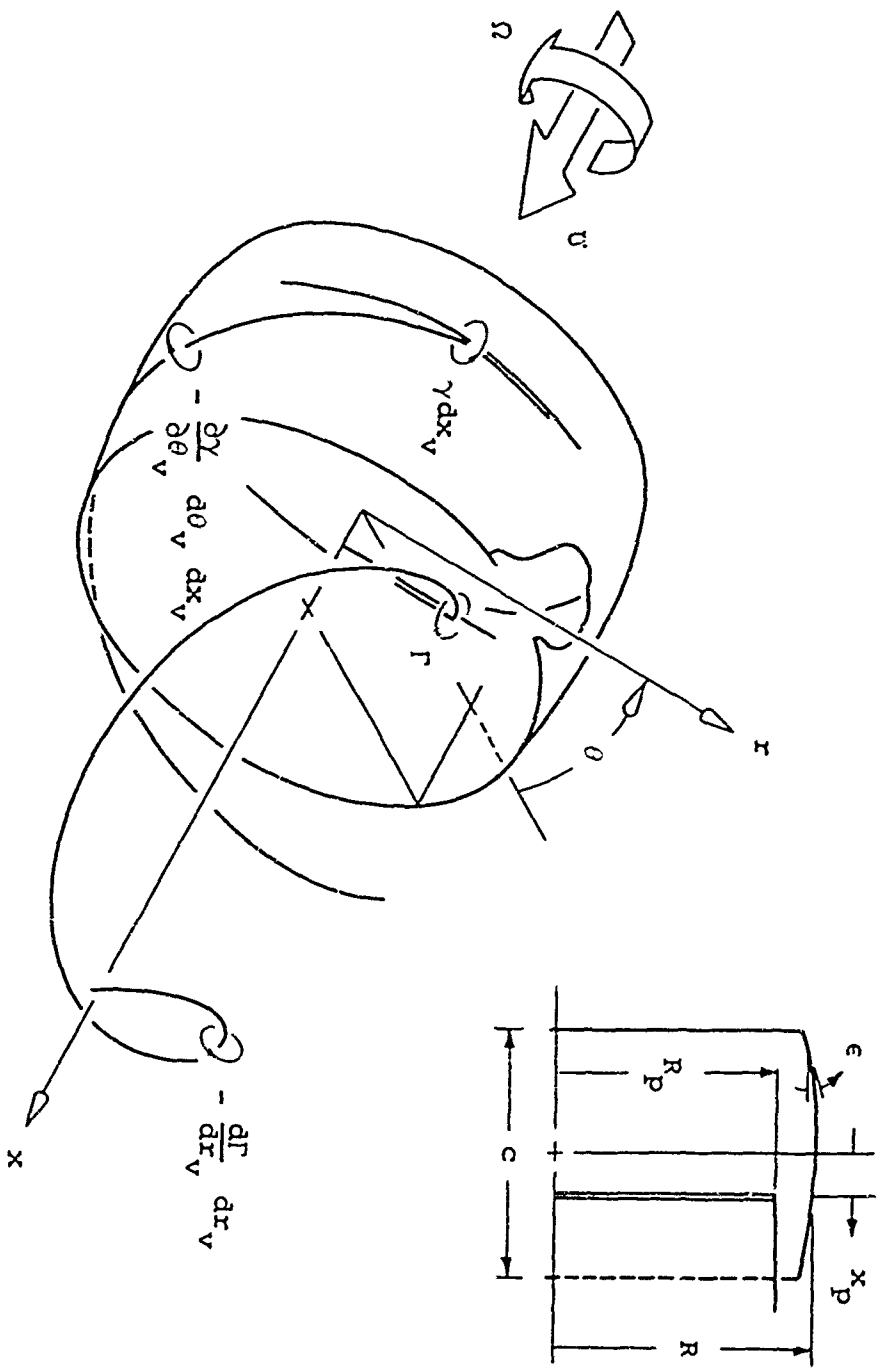


FIGURE 1.1

VORTEX SYSTEM AND GEOMETRY FOR DUCTED PROPELLER CONFIGURATION

1.2 Boundary Conditions and Vortex Model

The flow field must necessarily satisfy the following tangent-flow condition on the shroud,

$$\tan \epsilon = \frac{v(x, r_s, \theta)}{U+u(x, r_s, \theta)} \quad (1.1)$$

where $\epsilon(x)$ and $r_s(x)$ denote the local inclination angle and radius of the shroud respectively. The components of the disturbance velocity induced by the propeller and duct u, v, w are defined in terms of the total velocity \underline{q} by

$$\underline{q} \equiv (U+u)\underline{i}_x + v\underline{i}_r + (\Omega r+w)\underline{i}_\theta \quad (1.2)$$

where $\underline{i}_x, \underline{i}_r, \underline{i}_\theta$ are axial, radial, and circumferential unit vectors respectively. With R defined as the duct radius at the propeller plane, it follows from our assumption of small camber that

$$\tan \epsilon = O(\epsilon)$$

$$\underline{q}(x, r_s, \theta) = \underline{q}(x, R, \theta)[1 + O(\epsilon)] \quad (1.3)$$

In addition, the magnitude of U lies between zero for the static case and $O(u, v, w)$ for low-speed flight. The linearized form of the tangent-flow condition may therefore be expressed simply as

$$0 = v(x, R, \theta) \quad (1.4)$$

To compute the disturbance flow, in particular the radial wash $v(x, R, \theta)$, we introduce a classical vortex model to represent the shroud and propeller as in the forward-flight case¹, see Fig. 1.1. That is, the shroud is replaced by a distribution of ring vortices of strength $\gamma(x_v, \theta_v)$ per unit axial length over the "mean" duct $r_v = R$, $-c/2 \leq x_v \leq c/2$, where the v subscripts will be used in referring to vortex elements. Conservation of vorticity requires that these bound vortices be accompanied by trailing vortices of elemental strength $-\partial\gamma/\partial\theta_v$. The propeller is represented by N bound radial vortex spikes of strength $\Gamma(r_v)$ over the blade radius, $0 \leq r_v \leq R_p$, together with their associated trailing vortices of strength $-\Gamma'(r_v)$ per unit radial length. Throughout, the prime will denote differentiation with respect to the indicated argument.

1.3 Evaluation of the Radial Wash

The radial wash $v(x, R, \theta)$ contains θ -harmonics of order $0, N, 2N, \dots$, each of which must satisfy Eq. (1.4). In seeking the zeroth harmonic of $\gamma(x_v, \theta_v)$, say $\gamma_0(x_v)$, let us consider the zeroth harmonic of Eq. (1.4),

$$0 = v_0(x, R) \quad (1.5)$$

We may express v_0 as the sum of four components: v_{γ_0} , v_{γ_0}' , v_{Γ_0} and v_{Γ_0}' , which represent the contributions from the bound and trailing shroud and propeller vortices respectively. These components can be expressed in terms of the unknown shroud loading γ and the given blade loading Γ by means of the Biot-Savart law.

This general procedure has been carried out in Chapter Two of Ref. 1. The components v_{γ_0} and v_{Γ_0} may be found, with slight changes in nomenclature, as the zeroth harmonics of " $\underline{q}_\gamma \cdot \underline{i}_r$ " and " $\underline{q}_\Gamma \cdot \underline{i}_r$ " respectively. We find that

$$v_{\gamma_0}(x, R) = -\frac{1}{2\pi R^2} \int_{-c/2}^{c/2} (x-x_v) Q_{\frac{1}{2}}'(\sigma_1) \gamma_0(x_v) dx_v \quad (1.6)$$

and

$$v_{\Gamma_0}(x, R) = 0 \quad (1.7)$$

where

$$\sigma_1 \equiv 1 + (x-x_v)^2/2R^2 \quad (1.8)$$

and $Q_{\frac{1}{2}}$ is the Legendre function of second kind and one-half order. The Legendre functions of second kind and general half-integer order have been tabulated in Ref. 8.

In computing v_{γ_0}' we see from the harmonic nature of the shroud trailing vortex system that

$$v_{\gamma_0}'(x, R) = 0 \quad (1.9)$$

In order to proceed with the evaluation of v_{Γ_0}' , it is necessary to know the geometry of the trailing propeller vortices. For any given blade this is determined by the trajectories of the fluid particles which pass over the blade and are convected downstream with the total local fluid velocity \underline{q} , given by Eq. (1.2). In the case of forward flight, the perturbational terms are negligible compared to U and Ωr so that within the confines of linear theory the trailing vortices were assumed to be regular helices with pitch determined by U and Ωr_v . In low-speed flight we may again neglect v and w . For w this is permissible because it is still quite small compared to Ωr . For v the justification follows from the twofold action of the shroud: First, by contributing an appreciable amount of thrust the shroud effectively reduces the required propeller disk loading, and hence the resulting slipstream contraction. Second and more important, slipstream contraction is inhibited by the shroud tangent-flow condition, particularly over the portion immediately downstream which, in fact, contributes most heavily to v_{Γ_0}' on the shroud. These arguments are substantiated by recent numerical results of H. R. Chaplin⁷ who computes ultimate contraction ratios of only a few percent.

Although we neglect v and w , we may not neglect u ,

which is of the same order as U for the low-speed flight condition. The axial component actually varies both axially and radially, resulting in deformed helices of non-constant pitch. This causes considerable complication. For simplicity, we will disregard any axial variation and approximate each trailing vortex as a regular helix of pitch $j(r)$. The appropriateness of this important assumption will be examined in some detail later and, for the present, we merely give the following motivation: For a free propeller, u increases monotonely from its value at the propeller plane to approximately twice that value in the ultimate wake, so that a constant-pitch assumption would clearly be inappropriate in the low-speed range. In the case of the ducted propeller, however, the duct induces an axial component which varies in a complementary fashion; that is, it decays from its value at the propeller plane to zero in the ultimate wake. As such it can be expected to remove much of the axial variation in pitch so that the pitch may, indeed, be sufficiently constant.

With these approximations, the appropriate expression for $v_{\Gamma'_0}$ on the shroud is given by Eq. (16) of Ref. 9, with suitable modification of nomenclature, as

$$v_{\Gamma'_0}(x, R) = \frac{N}{4\pi^2 R_p \sqrt{R}} \int_0^{R_p} \frac{Q_{\frac{1}{2}}(\sigma_2) \sqrt{r_v}}{j(r_v)} \Gamma'(r_v) dr_v \quad (1.10)$$

where

$$\sigma_2 \equiv 1 + [(x-x_p)^2 + (R-r_v)^2]/2Rr_v \quad (1.11)$$

and j is the local pitch, as yet undetermined.

1.4 The Resulting Integral Equation

Inserting Eqs. (1.6), (1.7), (1.9) and (1.10) into the tangent-flow condition Eq. (1.5) results in the following integral equation in non-dimensional form for γ_0 ,

$$\begin{aligned} \frac{N}{4\pi^2} \int_0^\mu \frac{Q_{\frac{1}{2}}(\sigma_2) \sqrt{\bar{r}_v}}{j(\bar{r}_v)} \bar{\Gamma}'(\bar{r}_v) d\bar{r}_v \\ = \frac{1}{2\pi} \int_{-\lambda}^\lambda (\bar{x}-\bar{x}_v) Q_{\frac{1}{2}}'(\sigma_1) \bar{\gamma}_0(\bar{x}_v) d\bar{x}_v \end{aligned} \quad (1.12)$$

With ΩR_p as our reference velocity instead of U , which may be zero, we have non-dimensionalized according to

$$\bar{x} \equiv x/R$$

$$\bar{r} \equiv r/R$$

$$\bar{\gamma}_0 \equiv \gamma_0/\Omega R_p$$

$$\bar{\Gamma} \equiv \Gamma/\Omega R_p^2 \quad (1.13)$$

and have introduced the geometric parameters

$$\mu \equiv R_p/R$$

$$\lambda \equiv c/2R \tag{1.14}$$

Comparing Eq. (1.12) with the corresponding forward-flight equation, see Eqs. (1.4) and (1.5) of Ref. 2, we observe a striking difference:

For a given duct of small geometric camber, the function $\epsilon(x)$ appears explicitly and plays a dominant part in the forward-flight equation, but disappears completely from the equivalent low-speed equation.

For practical purposes this offers a tremendous simplification since the solution will be independent of $\epsilon(x)$ and will depend only on discrete parameters.

CHAPTER TWO

SOLUTION OF THE INTEGRAL EQUATION

2.1 High Blade-Number Limitation

Despite the absence of the geometric camber, we point out that if j is regarded as a known function then Eq. (1.12) is of the same mathematical form as the forward-flight equation which has already been inverted in closed form².

But how is j determined? We could, for example, take j equal to its actual value at the propeller plane, say j_p . Unfortunately, the latter depends in part upon u_γ and $u_{\gamma'}$. These velocities are functionals of γ_0 so that the integral equation is nonlinear. Since they are functionals of the higher harmonics γ_{mN} as well, the integral equation is also coupled with the higher harmonic integral equations. This situation appears to be intractable.

Instead, suppose we take j equal to its actual value in the ultimate wake, say j_∞ . This value still depends upon $u_{\gamma'}$, whereas u_γ tends to zero at infinity and is not involved. The velocity $u_{\gamma'}$ is a complicated functional of the higher harmonics γ_{mN} , but is independent of γ_0 so that the resulting integral equation is linear. However, the coupling remains. It appears that the only hope of arriving at a tractable situation is in further assuming the blade number to be

infinite, thus forcing u_{γ} , and hence the coupling, to zero. This restriction is imposed for the sake of mathematical rigor; practically, we would expect the results to be quite valid for blade numbers as low as 3 or 4.

2.2 Determination of Pitch

To evaluate $j_{\infty}(\bar{r})$ we note that u_{Γ} is identically zero, and write

$$j_{\infty} = \frac{U + u_{\Gamma}'}{\Omega R_p} = J + \bar{u}_{\Gamma}' \quad (2.1)$$

where \bar{u}_{Γ}' is evaluated at $x = \infty$.

To deal with the \bar{u}_{Γ}' term, we must specify the blade circulation $\bar{\Gamma}(\bar{r})$. As in the case of forward flight¹, we choose a distribution such that the Betz displacement condition is satisfied in the ultimate wake. For our case of high blade number the Betz condition requires a uniform jet velocity at $x = \infty$. It follows that \bar{u}_{Γ}' in Eq. (2.1), and hence j_{∞} , must be constant. From Eq. (22) of Ref. 9 we have at $x = \infty$,

$$\bar{u}_{\Gamma}' = \begin{cases} 0 & , \quad \bar{r} > \mu \\ \frac{N\bar{\Gamma}(\bar{r})}{2\pi j_{\infty}} & , \quad \bar{r} < \mu \end{cases} \quad (2.2)$$

and since both \bar{u}_{Γ}' and j_{∞} are to be independent of \bar{r} in the ultimate wake, we must have $\bar{\Gamma}(\bar{r})$ equal to a constant,

say $\bar{\Gamma}$. This means that all the trailing vorticity is concentrated on the slipstream surface $\bar{r} = \mu$. The pertinent value of $\bar{u}_{\Gamma'}$ to be used in Eq. (2.1) is therefore the value on the slipstream. Unfortunately, this value is not available from Eq. (2.2). Instead, we proceed by computing the propeller thrust T in two different ways:

First define the propeller thrust coefficient,

$$C_T \equiv T / \frac{1}{2} \rho (\Omega R_p)^2 (\pi R_p^2) \quad (2.3)$$

From the Kutta-Joukowski relation, consistent with our assumption that $w \ll \Omega r$, we have

$$C_T = \rho \int_0^{R_p} \Omega r N \Gamma \, dr / \frac{1}{2} \pi \rho \Omega^2 R_p^4 = \frac{N \bar{\Gamma}}{\pi} \quad (2.4)$$

On the other hand, momentum considerations lead to

$$C_T = (J + \bar{u}_{\Gamma'})^2 - J^2 \quad (2.5)$$

where $\bar{u}_{\Gamma'}$ here denotes the value inside the jet at $x = \infty$, or $C_T/2j_\infty$ according to Eqs. (2.2) and (2.4). The resulting Eq. (2.5) may be solved explicitly for j_∞ and we find that

$$j_\infty = \frac{1}{2} [J + \sqrt{C_T + J^2}] \quad (2.6)$$

Using this result in Eq. (2.1), we find as we might suspect that the appropriate value of \bar{u}_T , on the slipstream must be the average of the "inner" and "outer" values, $C_T/4j_\infty$.

It is convenient, at this point, to give precise definitions of the so-called "high-" and "low-" speed flight conditions. Roughly speaking, high-speed flight (also called "forward flight" or "cruise") corresponds to large J and small C_T . In the limiting case we have from Eq. (2.6) that $j_\infty \rightarrow J$, and so a measure of our "closeness" to ideal forward flight is the closeness of j_∞/J to unity. Observing from Eq. (2.6) that

$$j_\infty/J \approx 1 + C_T/4J^2 \quad (2.7)$$

we have $C_T/4J^2 \ll 1$ as our criterion. Analogously, $j_\infty \rightarrow \sqrt{C_T}/2$ in the low-speed limit, and

$$j_\infty/(\sqrt{C_T}/2) \approx 1 + J/\sqrt{C_T} \quad (2.8)$$

Our criterion for low-speed flight may therefore be stated as $J/\sqrt{C_T} \ll 1$. Both conditions may be given in terms of a single "flight parameter" $\delta \equiv J/\sqrt{C_T}$, as

$$\begin{aligned} \text{HIGH-SPEED:} & \quad 1/4\delta^2 \ll 1 \\ \text{LOW-SPEED:} & \quad \delta \ll 1 \end{aligned} \quad (2.9)$$

2.3 Solution of the Integral Equation

With $\bar{\Gamma}(\bar{r})$ constant and $j(\bar{r})$ given by j_∞ of Eq. (2.6), the integral equation reduces to

$$-\frac{\mu^{1/2} C_T}{4\pi j_\infty} Q_{1/2}(\sigma_3) = \frac{1}{2\pi} \int_{-\lambda}^{\lambda} (\bar{x} - \bar{x}_v) Q_{1/2}'(\sigma_1) \bar{\gamma}(\bar{x}_v) d\bar{x}_v \quad (2.10)$$

with

$$\sigma_3 \equiv 1 + [(\bar{x} - \bar{x}_p)^2 + (1 - \mu)^2] / 2\mu \quad (2.11)$$

In addition, we have dropped the zero subscript on $\bar{\gamma}$ since we have forced the higher harmonics to zero.

Following Ref. 2, we introduce a new axial coordinate ϕ such that

$$\bar{x} \equiv -\lambda \cos \phi \quad (2.12)$$

and seek a Glauert series solution of the form

$$\bar{\gamma} = g_0 \cot \frac{\phi}{2} + \sum_{n=1}^{\infty} g_n \sin n\phi \quad (2.13)$$

If we express

$$Q_{1/2}(\sigma_3) \equiv q_0 - \sum_{n=1}^{\infty} q_n \cos n\phi \quad (2.14)$$

for convenience, the solution is given in matrix form as

$$\{g\} = \frac{\mu^{\frac{1}{2}} c_T}{2\pi j_\infty} [I-P]^{-1} \{q\} \quad (2.15)$$

where $\{g\}$ and $\{q\}$ denote the infinite column vectors

$$\{g\} \equiv \begin{Bmatrix} g_0 \\ g_1 \\ g_2 \\ \vdots \\ \vdots \\ \vdots \end{Bmatrix} \quad \{q\} \equiv \begin{Bmatrix} q_0 \\ q_1 \\ q_2 \\ \vdots \\ \vdots \\ \vdots \end{Bmatrix} \quad (2.16)$$

$[I]$ being the identity matrix, with unity for each element on the main diagonal and zero for every other element, and $[P]$ the "curvature matrix" of Ref. 2, the elements of which depend upon λ and tend to zero in the two-dimensional limit of $\lambda \rightarrow 0$.

It has been shown² that the Neumann expansion

$$[I-P]^{-1} = [I] + [P] + [P]^2 + \dots \quad (2.17)$$

is valid for all finite values of λ . The inverse matrix has been evaluated³ accordingly for $\lambda = 0.25, 0.50, 0.75$ and 1.0, and is reproduced here, except for $\lambda = 1.0$, in

Tables 1.1 - 1.3 .

The $q_n(\lambda, \mu, \bar{x}_p)$'s have been evaluated numerically to within ± 0.001 and are tabulated for $n = 0, 1, 2, \dots, 12$; $\lambda = 0.25, 0.375, 0.50, 0.625, 0.75$; $\mu = 0.90, 0.94, 0.97, 1.0$; and $x_p/c = 0.0, \pm 0.125, \pm 0.25, \pm 0.375$, in Tables 2.1 - 2.5 . The "in-between" values, $\lambda = 0.375$ and 0.625 , were included to retain a consistent degree of accuracy in interpolation, and the value $\mu = 1.0$ to facilitate interpolation for cases of small tip clearance.

In summary then, the static and low-speed solution is given by Eq. (2.13) together with Eq. (2.15) and Tables 1.1 - 2.5 , cf. the forward-flight solution².

CHAPTER THREE

SHROUD SURFACE PRESSURES AND THRUST

3.1 Shroud Surface Pressures

We define the shroud surface pressure coefficient, based upon the propeller tip speed, as

$$c_p \equiv \frac{p - p_\infty}{\frac{1}{2} \rho (\Omega R_p)^2} \quad (3.1)$$

where p and p_∞ are the static pressures on the shroud and at infinity respectively. From Bernoulli's equation we have

$$p - p_\infty = - \frac{1}{2} \rho [(U+u)^2 - U^2] \quad (3.2)$$

since $v \approx 0$, and Eq. (3.1) becomes

$$c_p = - (2J + \bar{u}) \bar{u} \quad (3.3)$$

We call attention to the nonlinear term \bar{u}^2 . For finite blade number the higher harmonics of \bar{u} would therefore contribute to the zeroth pressure harmonic since terms of the form $\cos^2 m\theta = (\frac{1}{2} + \frac{1}{2} \cos 2m\theta)$ and $\sin^2 m\theta = (\frac{1}{2} - \frac{1}{2} \cos 2m\theta)$ contain axisymmetric portions. This coupling with the higher harmonics in the zeroth pressure harmonic would be in addition

to the coupling of the governing integral equations, discussed above in Section 2.1, and once again emphasizes the need to limit our attention to high blade numbers.

Now, on the shroud \bar{u} is equal to the sum of \bar{u}_γ and $\bar{u}_{\Gamma'}$. By means of a careful limiting process it may be shown, see Eq. (1.10) of Ref. 3, that

$$\bar{u}_\gamma(\bar{x}, 1^\pm) = \bar{r} \frac{\bar{\gamma}(\bar{x})}{2} + \frac{1}{2\pi} \int_{-\lambda}^{\lambda} [Q'_{\frac{1}{2}}(\sigma_1) - Q'_{-\frac{1}{2}}(\sigma_1)] \bar{\gamma}(\bar{x}_v) d\bar{x}_v \quad (3.4)$$

The first term on the right hand side represents the well-known two-dimensional contribution, and the second term supplies the effect of three-dimensionality. From Hough again, we may express \bar{u}_γ conveniently as

$$\bar{u}_\gamma(\bar{x}, 1^\pm) = \bar{r} \frac{g_0}{2} \cot \frac{\phi}{2} + \bar{r} \sum_{n=1}^{\infty} \frac{g_n}{2} \sin n\phi + \frac{1}{2} \{\phi\}^T \{s\} \{g\} \quad (3.5)$$

where the $[s(\lambda)]$ matrix is tabulated in Ref. 3 and reproduced here in Tables 3.1 - 3.3 for $\lambda = 0.25, 0.50,$ and 0.75 . The transpose $\{\phi\}$ vector is defined as

$$\{\phi\}^T \equiv \frac{1}{2} (1, -\cos\phi, -\cos 2\phi, \dots) \quad (3.6)$$

Turning to $\bar{u}_{\Gamma'}$, we find, from Eq. (28) of Ref. 9,

$$\bar{u}_{\Gamma'}(\bar{x}, 1) = \frac{c_T}{8\pi j_\infty} \left[\frac{\bar{x} - \bar{x}_p}{\sqrt{\mu}} Q_{\frac{1}{2}}(\sigma_3) - \pi \Lambda_0(\beta, \kappa) \right] \quad (3.7)$$

where $\Lambda_0(\beta, \kappa)$ is Heuman's lambda function with argument β and modulus κ defined as

$$\beta \equiv \sin^{-1} \frac{\bar{x} - \bar{x}_p}{[(\bar{x} - \bar{x}_p)^2 + (1 - \mu)^2]^{\frac{1}{2}}}, \quad \kappa \equiv \left[\frac{4\mu}{(\bar{x} - \bar{x}_p)^2 + (1 + \mu)^2} \right]^{\frac{1}{2}} \quad 3. \quad (3.8)$$

This function was tabulated in Ref. 10, and a shorter tabulation appears in Ref. 11. For μ and \bar{x}_p in the range of practical interest κ is slightly less than or equal to unity over the shroud, and the simple approximation

$$\Lambda_0(\beta, \kappa) \approx \Lambda_0(\beta, 1) = 2\beta/\pi \quad (3.9)$$

is sufficiently accurate.

With \bar{u} computed as the sum of \bar{u}_γ and $\bar{u}_{\Gamma'}$, from Eqs. (3.5) and (3.7), the pressure coefficient on the shroud is then given by Eq. (3.3). In addition we may compute the net surface pressure coefficient, $c_p] \equiv c_p(\bar{x}, 1^-) - c_p(\bar{x}, 1^+)$, as

$$c_p] = - \left\{ 2J + \{\phi\}^T [s] \{g\} + \frac{c_T}{4\pi j_\infty} \left[\frac{\bar{x} - \bar{x}_p}{\sqrt{\mu}} Q_{\frac{1}{2}}(\sigma_3) - 2\beta \right] \right\} \bar{\gamma} \quad (3.10)$$

The first term $-2J\bar{\gamma}$ coincides with the corresponding

forward-flight result, and the additional two terms represent the nonlinear contributions. Physically, Eq. (3.10) expresses the Kutta-Joukowski interaction between the axial velocity and the bound shroud circulation.

3.2 Shroud Thrust

From Lagally's extension of the general Kutta-Joukowski formula, the elemental thrust dt , positive upstream, on a shroud ring vortex of strength γdx_v is¹²

$$dt = -\rho(v_{\Gamma'}) (2\pi R \gamma dx_v) \quad (3.11)$$

Defining the shroud thrust coefficient as

$$C_t \equiv t / \frac{1}{2} \rho (\Omega R_p)^2 (\pi R_p^2) \quad (3.12)$$

We find, with $\bar{v}_{\Gamma'}$ from the left side of Eq. (2.10), and $\bar{\gamma}$ and $Q_{\frac{1}{2}}$ from Eqs. (2.13) and (2.14) respectively, that

$$\begin{aligned} C_t &= \frac{C_T}{\pi j_{\infty} \mu^{3/2}} \int_{-\lambda}^{\lambda} Q_{\frac{1}{2}}(\sigma_3) \bar{\gamma} d\bar{x}_v \\ &= \frac{\lambda C_T}{4 j_{\infty} \mu^{3/2}} \left[4q_0 g_0 + 2q_0 g_1 - 3q_1 g_0 - \sum_{n=1}^{\infty} q_n (g_{n+1} - g_{n-1}) \right] \end{aligned} \quad (3.13)$$

If we express the q_n 's in terms of the g_n 's by

means of Eq. (2.15) and recall the properties of the [P] matrix from Section 2.2 of Ref. 2, we find that C_t reduces to the single term

$$C_t = \frac{2\pi\lambda}{\mu^2} g_0^2 \quad (3.14)$$

This we recognize immediately as the classical leading-edge suction force. It is not unexpected, of course, since $\bar{\gamma}$ is independent of the geometric shroud camber in the present theory. In other words, the shroud thrust is the same as if the camber were identically zero, in which case the only possible axial force is the leading-edge suction force. This result was anticipated several years ago by A. H. Sacks, in a private communication, based upon physical reasoning.

CHAPTER FOUR

INVESTIGATION OF CONSTANT-PITCH HYPOTHESIS

4.1 Pitch Iteration

To investigate the degree of validity of the constant-pitch assumption, we will set up an iterative solution which, in the limit, is expected to yield the exact pitch distribution including the axial variation. At the same time, it should also provide considerable physical insight into the problem.

If we take as our initial value $j^{(0)} = j_\infty$, that is $\bar{u}_\Gamma^{(0)} = c_T/4j_\infty$ and $\bar{u}_\gamma^{(0)} = 0$, we find the resulting shroud loading $\gamma^{(0)}$ explicitly from Eq. (2.15). With this known, we may compute a new pitch distribution $j^{(1)}(\bar{x})$ according to

$$j^{(1)}(\bar{x}) = J + \bar{u}_\gamma^{(1)}(\bar{x}, \mu) + \bar{u}_\Gamma^{(1)}(\bar{x}, \mu) \quad , \quad \bar{x}_p \leq \bar{x} < \infty \quad (4.1)$$

where $\bar{u}_\Gamma^{(1)}(\bar{x}, \mu)$ is taken as the average of the "inner" and "outer" values as before. Integration of $\bar{\gamma}^{(0)}$ over the shroud yields, cf. Eq. (32) of Ref. 9 ,

$$\bar{u}_\gamma^{(1)}(\bar{x}, \mu) = \frac{1}{2\pi\mu} \int_{-\lambda}^{\lambda} [\mu^{\frac{1}{2}} Q_{\frac{1}{2}}'(\sigma_4) - \mu^{-\frac{1}{2}} Q_{-\frac{1}{2}}'(\sigma_4)] \bar{\gamma}^{(0)}(\bar{x}_v) d\bar{x}_v \quad (4.2)$$

where

$$\sigma_4 \equiv 1 + [(\bar{x} - \bar{x}_v)^2 + (1 - \mu)^2] / 2\mu \quad (4.3)$$

The propeller-induced contribution may be found from Eq. (28) of Ref. 9 . After averaging and changing nomenclature, we have

$$\bar{u}_{\Gamma}^{(1)}(\bar{x}, \mu) = \frac{C_T}{8\pi j_{\infty}} \left[\pi + \frac{\bar{x} - \bar{x}_p}{\mu} Q_{-\frac{1}{2}}(\sigma_5) \right] \quad (4.4)$$

where

$$\sigma_5 \equiv 1 + (\bar{x} - \bar{x}_p)^2 / 2\mu^2 \quad (4.5)$$

If the right hand side of Eq. (4.2) is integrated numerically, then $j^{(1)}(\bar{x})$ is determined at any \bar{x} location. In the limit as $\bar{x} \rightarrow \infty$, $\bar{u}_{\gamma}^{(1)} \rightarrow 0$ and $\bar{u}_{\Gamma}^{(1)} \rightarrow C_T / 4j_{\infty}$ so that $j^{(1)}(\bar{x}) \rightarrow j_{\infty}$.

With the new trailing vortex geometry thus specified, the next step is to compute the corresponding propeller-induced radial wash $v_{\Gamma}^{(1)}$ on the shroud, and hence the new shroud vortex loading $\gamma^{(1)}$. Carrying this out, we find the result is equivalent to the integration over a semi-infinite cylinder of ring vortices of strength per unit length $N\Gamma / 2\pi R_p j^{(1)}(\bar{x}_v)$,

$$\bar{v}_{\Gamma}^{(1)}(\bar{x}) = - \frac{C_T}{4\pi\mu^{\frac{1}{2}}} \int_{\bar{x}_p}^{\infty} \frac{\bar{x} - \bar{x}_v}{j^{(1)}(\bar{x}_v)} Q_{\frac{1}{2}}'(\sigma_4) d\bar{x}_v \quad (4.6)$$

For practical purposes we split the integration into two ranges: the first from \bar{x}_p to \bar{X} , and the second from \bar{X} to ∞ . We choose \bar{X} large enough so that $j^{(1)}(\bar{x})$ may be approximated

by j_∞ in the latter "tail" portion. The integration in this portion may therefore be performed analytically, and

$$\begin{aligned} \bar{v}_\Gamma^{(1)}(\bar{x}) \approx & -\frac{C_T}{4\pi\mu^{\frac{1}{2}}} \int_{\bar{x}_p}^{\bar{x}} \frac{\bar{x}-\bar{x}_v}{j^{(1)}(\bar{x}_v)} Q_{\frac{1}{2}}'(\sigma_4) d\bar{x}_v \\ & -\frac{\mu^{\frac{1}{2}}C_T}{4\pi j_\infty} Q_{\frac{1}{2}} \left[1 + \frac{(\bar{x}-\bar{X})^2 + (1-\mu)^2}{2\mu} \right] \end{aligned} \quad (4.7)$$

cf. the left hand side of Eq. (2.10) with \bar{x}_p replaced by \bar{X} .

We may now determine $\gamma^{(1)}$. Recalling again the left hand side of Eq. (2.10), or

$$\bar{v}_\Gamma^{(0)}(\bar{x}) = -\frac{\mu^{\frac{1}{2}}C_T}{4\pi j_\infty} Q_{\frac{1}{2}}(\sigma_3) \quad (4.8)$$

as well as Eqs. (2.14) and (2.15), we see that if we expand

$$-\frac{4\pi j_\infty}{\mu^{\frac{1}{2}}C_T} \bar{v}_\Gamma^{(1)} \equiv q_0^{(1)} - \sum_{n=1}^{\infty} q_n^{(1)} \cos n\phi \quad (4.9)$$

then $\gamma^{(1)}$ is given by

$$\{g^{(1)}\} = \frac{\mu^{\frac{1}{2}}C_T}{2\pi j_\infty} [I-P]^{-1}\{q^{(1)}\} \quad (4.10)$$

and the Glauber series of Eq. (2.13) with $g_0^{(1)}$ instead of

g_0 and so forth.

This process may be repeated. The only change necessary is in the evaluation of \bar{u}_r . Since the pitch is no longer constant, Eq. (4.4) does not apply. For $\bar{u}_r^{(2)}$ and all subsequent iterates, we have the analogous form to Eq. (4.6) for the radial component, namely

$$\bar{u}_r^{(2)}(\bar{x}, \mu) = \frac{C_T}{4\pi\mu} \int_{\bar{x}_p}^{\infty} \frac{1}{j^{(1)}(\bar{x}_v)} [Q'_{\frac{1}{2}}(\sigma_6) - Q'_{-\frac{1}{2}}(\sigma_6)] d\bar{x}_v \quad (4.11)$$

where

$$\sigma_6 \equiv 1 + (\bar{x} - \bar{x}_v)^2 / 2\mu^2 \quad (4.12)$$

4.2 Illustrative Results

We have carried out the above process on the CDC 1604 at the Cornell University Computing Center for the typical case

$$\begin{aligned} J &= 0 \\ C_T &= 0.1 \\ \lambda &= 0.5 \\ \mu &= 0.9 \\ \bar{x}_p &= 0 \end{aligned} \quad (4.13)$$

which will be considered further in the next chapter. Here we are only concerned with the iteration. The static case was chosen since it is the most critical; that is, the pitch hypothe-

sis can be expected to be least accurate at the static condition and to become more accurate as the flight speed is increased.

The results are shown for a two-step iteration in Fig. 4.1 . We see immediately that the axial variation of \bar{u}_γ and \bar{u}_Γ are quite "complementary", resulting in a reasonably constant pitch distribution. We also see from a comparison of $\bar{v}_\Gamma^{(0)}$ and $\bar{v}_\Gamma^{(1)}$ that, qualitatively, the effect of the axial variation in pitch is to shift the "effective" propeller plane rearward by approximately 2% of the chordlength.

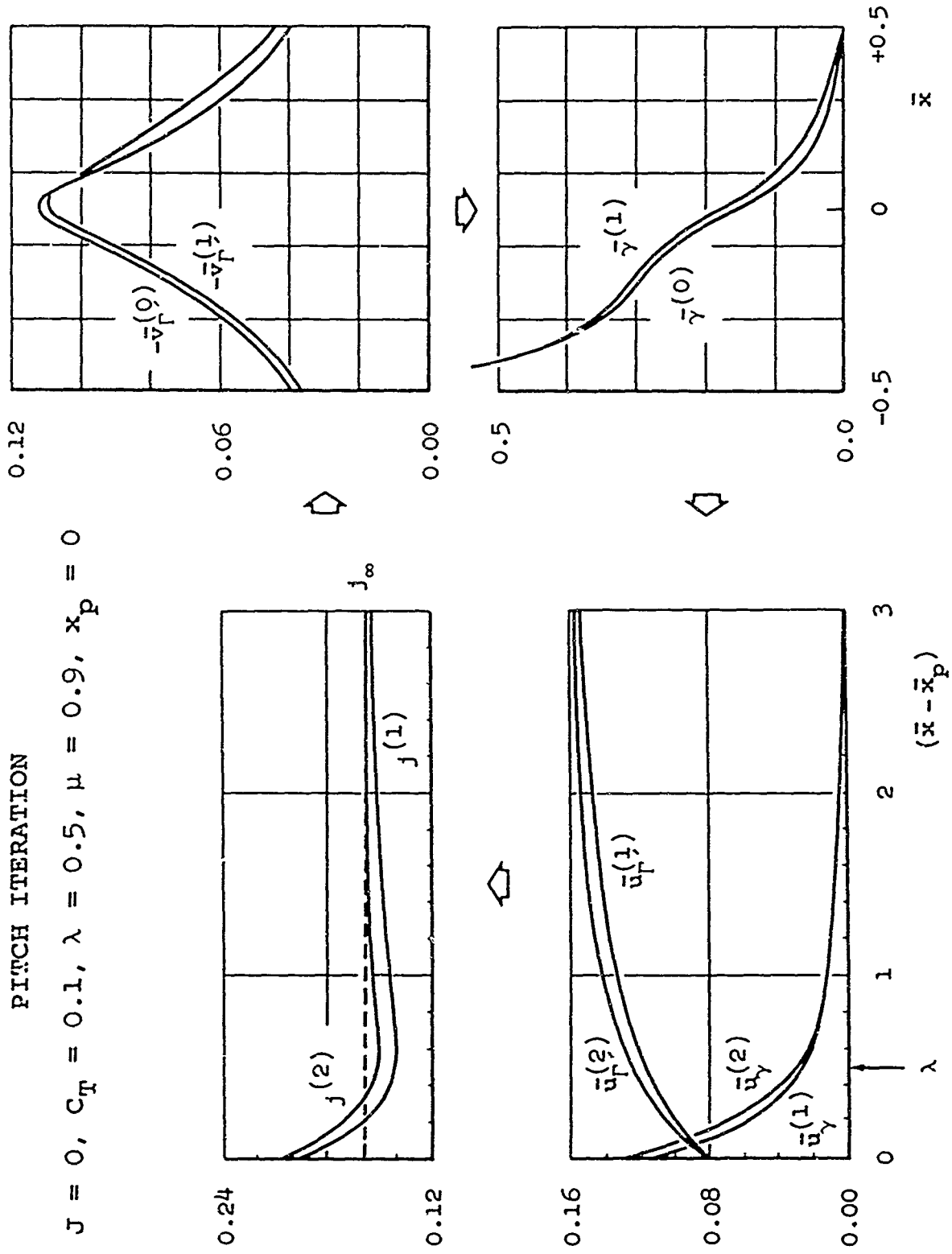
In judging the validity of the constant-pitch assumption, however, we are not concerned with the discrepancy between $j(x)$ and j_∞ per se but rather with the resulting discrepancy in the final quantities of interest, such as the shroud loading $\bar{\gamma}$ and the shroud thrust C_t . Truncating the Glauert series at $n=12$, the coefficients of $\bar{\gamma}^{(0)}$ and $\bar{\gamma}^{(1)}$ are given by

$$\{g^{(0)}\} = \left\{ \begin{array}{c} 0.1349 \\ 0.0215 \\ 0.0631 \\ -0.0001 \\ -0.0214 \\ 0.0000 \\ 0.0096 \\ 0.0000 \\ -0.0049 \\ 0.0000 \\ 0.0026 \\ 0.0000 \\ -0.0014 \end{array} \right\} \quad \{g^{(1)}\} = \left\{ \begin{array}{c} 0.1365 \\ 0.0348 \\ 0.0623 \\ -0.0065 \\ -0.0191 \\ 0.0019 \\ 0.0078 \\ -0.0005 \\ -0.0039 \\ 0.0002 \\ 0.0022 \\ -0.0001 \\ -0.0012 \end{array} \right\} \quad (4.14)$$

FIGURE 4.1

PITCH ITERATION

$J = 0, C_T = 0.1, \lambda = 0.5, \mu = 0.9, x_p = 0$



and $\bar{\gamma}^{(0)}$ and $\bar{\gamma}^{(1)}$ are compared in Fig. 4.1 . While the relative differences in some of the coefficients are appreciable, $\bar{\gamma}^{(0)}$ agrees with $\bar{\gamma}^{(1)}$ quite closely. Furthermore, $g^{(0)}$ and $g^{(1)}$ differ by only 1% so that, according to Eq. (3.13), $c_t^{(0)}$ and $c_t^{(1)}$ differ by only 2% .

CHAPTER FIVE
NUMERICAL EXAMPLES

5.1 Input Data

Let us consider the static case $J = 0$ with the following typical values for the parameters,

$$\begin{aligned}C_T &= 0.1 \\ \lambda &= 0.5 \\ \mu &= 0.9 \\ x_p/c &= 0.0 , -0.25\end{aligned}\tag{5.1}$$

where the first case, for $x_p/c = 0.0$, is identical to the one considered above in Section 4.2. The camber is assumed to be small, but arbitrary, since it has no effect in the present theory.

5.2 Results

In order to determine the shroud surface pressure coefficient and the shroud thrust, we first compute the vortex loading $\bar{\gamma}$. We find $\{g\}$ from Eq. (2.15) and Tables 1.2 and 2.3. For $x_p/c = 0.0$ the result is given by the first of Eqs. (4.14) and is reproduced below for convenience, together with the result for $x_p/c = -0.25$,

$$\{g\} = \left\{ \begin{array}{c} 0.1349 \\ 0.0215 \\ 0.0631 \\ -0.0001 \\ -0.0214 \\ 0.0000 \\ 0.0096 \\ 0.0000 \\ -0.0049 \\ 0.0000 \\ 0.0026 \\ 0.0000 \\ -0.0014 \end{array} \right\} , \left\{ \begin{array}{c} 0.1327 \\ -0.0499 \\ 0.0312 \\ 0.0317 \\ 0.0087 \\ -0.0069 \\ -0.0081 \\ -0.0023 \\ 0.0023 \\ 0.0027 \\ 0.0008 \\ -0.0009 \\ -0.0011 \end{array} \right\} \quad (5.2)$$

respectively. The corresponding $\bar{\gamma}$'s are computed from Eq. (2.13) and plotted in Fig. 5.1 .

The inner and outer shroud surface pressures are then calculated from Eqs. (3.3), (3.5), (3.6), (3.7), (3.8), (3.9) and Table 3.2 , and the results are shown in Fig. 5.2 . Two striking features of these curves are apparent: first, the outer surface pressure distribution is virtually independent of the propeller position and, second, the inner surface pressure coefficient decays to zero almost immediately downstream of the propeller plane. This lack of "communication", expressed by the first result, is not unexpected, on physical grounds. Regarding the second result, we find that on the inner surface \bar{u}_r and \bar{u}_y are additive upstream of the propeller plane, whereas they oppose each other downstream of it.

Consequently, it is natural to wonder whether, for practical purposes, we may replace the two parameters λ and \bar{x}_p by the single parameter $(\bar{x}_p + \lambda)$; that is, the nondimensional distance from the leading edge to the propeller plane. The results of sample calculations, however, are found to differ significantly so that the above simplification is not valid.

Finally, from Eq. (3.13), the shroud-to-propeller thrust ratio obtained for the two cases of Eqs. (4.13) and (5.1) are

$$c_t/c_T = \begin{matrix} 0.683 & , & x_p/c = -0.25 \\ 0.706 & , & x_p/c = 0.0 \end{matrix} \quad (5.3)$$

The closeness of these two results seems to support Kriebel's a priori assumption^{5,6} that c_t/c_T is independent of x_p/c . But we emphasize that this is not the case, even in an approximate sense, for the detailed shroud surface-pressure distribution, see Fig. 5.2 .

5.3 Comparison with Experiment

Although the present theory is incomplete in the sense that the effects of shroud thickness are not yet incorporated, it is nevertheless of interest to compare it with experiment. In the absence of suitable detailed surface pressure measurements, we are limited to only a gross comparison based upon the shroud thrust. If we use the inner shroud radius at the pro-

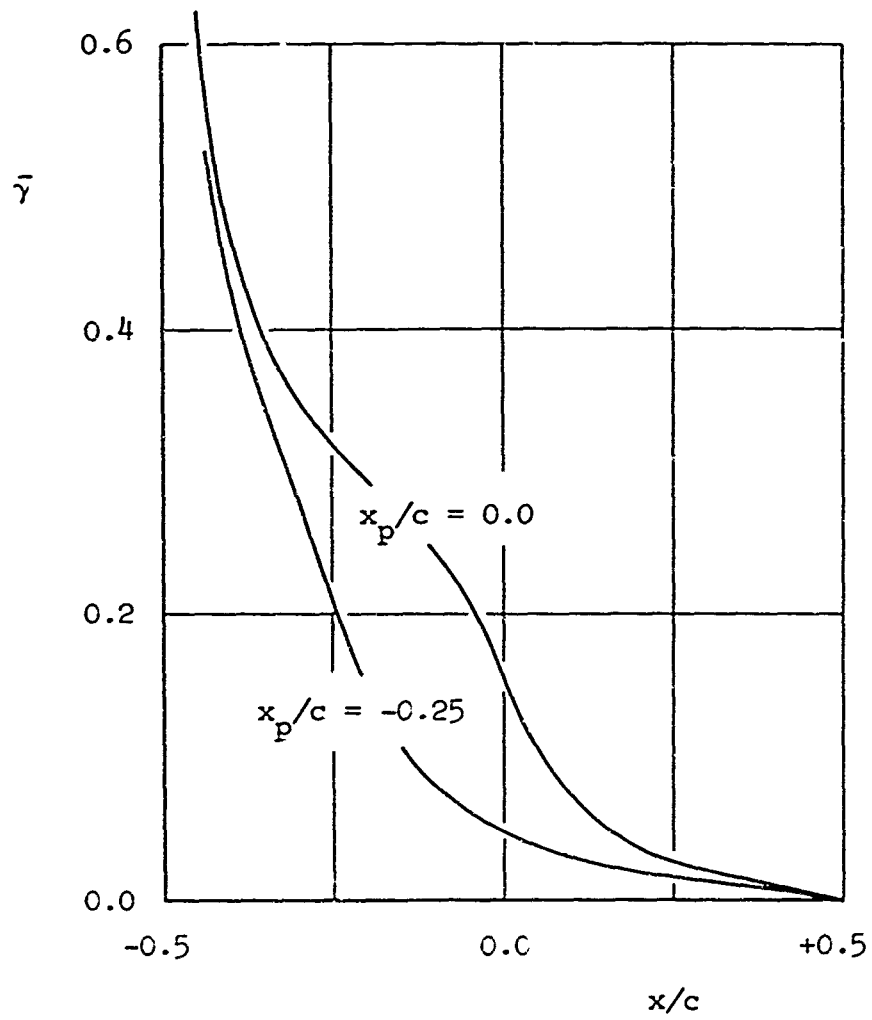


FIGURE 5.1

CHORDWISE VARIATION OF $\bar{\gamma}$

$$J = 0, c_T = 0.1, \lambda = 0.5, \mu = 0.9$$

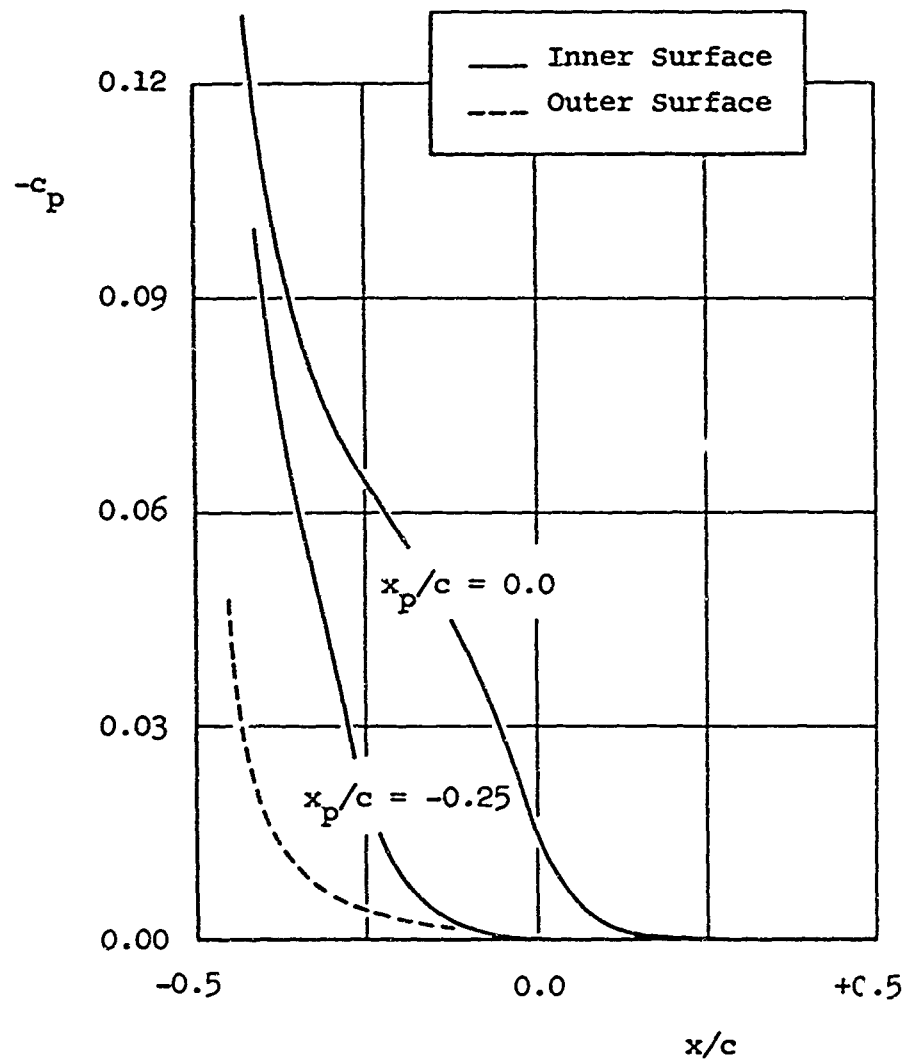


FIGURE 5.2

CHORDWISE VARIATION OF c_p

$$J = 0, c_T = 0.1, \lambda = 0.5, \mu = 0.9$$

pellor plane, comparison with the results of K. J. Grunwald and K. W. Goodson¹³ where $J = 0$, $\lambda = 0.620$, $x_p/c = -0.146$ and $\mu = 0.995$, gives a predicted value of C_t which is about 30% lower than their measured value. Since C_t is a second-order quantity, though, the corresponding error in the shroud circulation is only half as great; i. e. about 15% , which is quite reasonable.

CONCLUSIONS

A theory has been developed for the steady aerodynamic loading on a ducted propeller with finite blade number in static and low-speed flight. For a shroud of small camber and zero thickness, we have shown that:

The effect of the geometric camber is of higher order and may be neglected.

The steady shroud circulation is coupled nonlinearly with the higher harmonics through the pitch of the propeller wake. This coupling imposes, in a rigorous sense, a high blade-number restriction.

An analytic solution together with simple expressions for the surface pressures and shroud thrust can be obtained, subject to a reasonable assumption of constant pitch for the trailing propeller vortices.

The pitch hypothesis may be dropped and an iterative solution pursued, but an illustrative calculation indicates that the corresponding final results do not differ significantly.

The outer shroud surface pressure is quite insensitive to the axial propeller position, and the inner shroud surface pressure decays almost to zero immediately behind the propeller plane.

Results of a limited comparison with experiment are quite reasonable.

It is anticipated that the contents of this report will be condensed and presented in a tabular format as a simple addition to the procedure of Ref. 4 .

REFERENCES

1. Ordway, D. E., Sluyter, M. M., and Sonnerup, B. U. O., Three-Dimensional Theory of Ducted Propellers, THERM, Incorporated, TAR-TR 602, August 1960.
2. Ordway, D. E., and Greenberg, M. D., General Harmonic Solutions for the Ducted Propeller, THERM, Incorporated, TAR-TR 613, August 1961.
3. Hough, G. R., The Aerodynamic Loading on Streamlined Ducted Bodies, THERM, Incorporated, TAR-TR 625, December 1962.
4. Kaskel, A. L., Ordway, D. E., Hough, G. R., Ritter, A., A Detailed Numerical Evaluation of Shroud Performance for Finite-Bladed Ducted Propellers, THERM, Incorporated, TAR-TR 639, December 1963.
5. Kriebel, A. R., Theoretical Investigation of Static Coefficients, Stability Derivatives, and Interference for Ducted Propellers, Itek Corp., Vidya Report No. 112, March 1964.
6. Kriebel, A. R., Theoretical Stability Derivatives for a Ducted Propeller, Journal of Aircraft, Vol. 1, No. 4, pp. 203-210, July-August, 1964.
7. Chaplin, H. R., A Method for Numerical Calculation of Slipstream Contraction of a Shrouded Impulse Disc in the Static Case With Application to Other Axisymmetric Potential Flow Problems, David Taylor Model Basin Report 1857, June 1964.
8. Sluyter, M. M., A Computational Program and Extended Tabulation of Legendre Functions of Second Kind and Half Order, THERM, Incorporated, TAR-TR 601, August 1960.
9. Hough, G. R., and Ordway, D. E., The Generalized Actuator Disk, Second Southeastern Conference on Theoretical and Applied Mechanics, Atlanta, Georgia, March 5-6, 1964; Proceedings to be published by Pergamon Press.
10. Heuman, C., Tables of Complete Elliptic Integrals, Journal of Mathematics and Physics, Vol. 20, pp. 127-206, 1941.

11. Byrd, P. F., and Friedman, M. D., Handbook of Elliptic Integrals for Engineers and Physicists, Springer-Verlag, Berlin, 1954.
 12. Wilson, D. H., Hydrodynamics, Edward Arnold, London, 1959.
 13. Grunwald, K. J., and Goodson, K. W., Aerodynamic Loads on an Isolated Shrouded-Propeller Configuration for Angles of Attack from -10° to 110° , NASA TN D-995, January 1962.
-

TABLES

	Page
1.1 ($[I] + [P] + [P]^2 + \dots$) Matrix for $\lambda = 0.25$	41
1.2 ($[I] + [P] + [P]^2 + \dots$) Matrix for $\lambda = 0.50$	42
1.3 ($[I] + [P] + [P]^2 + \dots$) Matrix for $\lambda = 0.75$	43
2.1 q_n Coefficients for $\lambda = 0.25$	44
2.2 q_n Coefficients for $\lambda = 0.375$	45
2.3 q_n Coefficients for $\lambda = 0.50$	46
2.4 q_n Coefficients for $\lambda = 0.625$	47
2.5 q_n Coefficients for $\lambda = 0.75$	48
3.1 $[s]$ Matrix for $\lambda = 0.25$	49
3.2 $[s]$ Matrix for $\lambda = 0.50$	50
3.3 $[s]$ Matrix for $\lambda = 0.75$	51

1.0277	0	0.0139	0	0.0000	0	0.0000
0.0568	1.0308	0.0008	-0.0031	0.0000	0.0000	0.0000
0.0063	0	1.0041	0	-0.0010	0	0.0000
-0.0001	-0.0010	0.0000	1.0015	0.0000	-0.0005	0.0000
0.0000	0	-0.0005	0	1.0008	0	-0.0003
0.0000	0.0000	0.0000	-0.0003	0.0000	1.0005	0.0000
0.0000	0	0.0000	0	-0.0002	0	1.0003

TABLE 1.1

([I] + [P] + [P]² + ...) MATRIX FOR λ = 0.25

1.0796	0	0.0400	0	-0.0002	0	0.0000
0.1719	1.0933	0.0064	-0.0138	0.0000	0.0001	0.0000
0.0274	0	1.0179	0	-0.0042	0	0.0000
-0.0009	-0.0046	0.0000	1.0062	0.0000	-0.0020	0.0000
-0.0002	0	-0.0021	0	1.0032	0	-0.0012
0.0000	0.0000	0.0000	-0.0012	0.0000	1.0020	0.0000
0.0000	0	0.0000	0	-0.0008	0	1.0013

TABLE 1.2

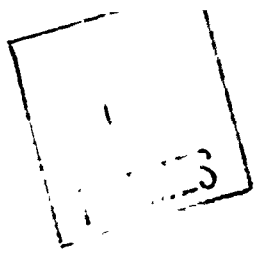
([I] + [P] + [P]² + ...) MATRIX FOR λ = 0.50

1.1398	0	0.0704	0	-0.0005	0	0.0000
0.3186	1.1722	0.0197	-0.0329	-0.0001	0.0004	0.0000
0.0650	0	1.0425	0	-0.0101	0	0.0001
-0.0022	-0.0110	-0.0001	1.0147	0.0000	-0.0047	0.0000
-0.0008	0	-0.0051	0	1.0074	0	-0.0028
0.0000	0.0001	0.0000	-0.0028	0.0000	1.0045	0.0000
0.0000	0	0.0000	0	-0.0018	0	1.0031

TABLE 1.3

$([I] + [P] + [P]^2 + \dots)$ MATRIX FOR $\lambda = 0.75$

BLANK PAGE



$$x_p/c = 0.0$$

$$x_p/c = \pm 0.125$$

n \ μ	$x_p/c = 0.0$				$x_p/c = \pm 0.125$			
	0.90	0.94	0.97	1.00	0.90	0.94	0.97	1.00
0	1.744	1.913	2.044	2.178	1.735	1.907	2.042	2.180
1	0	0	0	0	± 0.293	± 0.363	± 0.422	± 0.484
2	0.440	0.603	0.769	0.982	0.383	0.523	0.667	0.858
3	0	0	0	0	∓ 0.128	∓ 0.213	∓ 0.313	∓ 0.457
4	-0.104	-0.192	-0.309	-0.499	-0.059	-0.104	-0.163	-0.265
5	0	0	0	0	± 0.049	± 0.110	± 0.205	± 0.381
6	0.032	0.080	0.162	0.333	0.005	0.008	0.011	0.018
7	0	0	0	0	∓ 0.017	∓ 0.051	∓ 0.118	∓ 0.280
8	-0.011	-0.037	-0.096	-0.250	0.003	0.013	0.039	0.109
9	0	0	0	0	± 0.005	± 0.020	± 0.057	± 0.169
10	0.004	0.019	0.060	0.200	-0.003	-0.013	-0.047	-0.163
11	0	0	0	0	∓ 0.001	∓ 0.005	∓ 0.017	∓ 0.064
12	-0.002	-0.010	-0.040	-0.167	0.001	0.009	0.037	0.166

TABLE 2.1

q_n COEFFICIENTS FOR

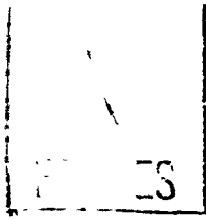
$$x_p/c = \pm 0.25$$

$$x_p/c = \pm 0.375$$

$x_p/c = \pm 0.25$				$x_p/c = \pm 0.375$			
0.90	0.94	0.97	1.00	0.90	0.94	0.97	1.00
1.705	1.887	2.033	2.185	1.639	1.832	2.003	2.193
± 0.557	± 0.703	± 0.831	± 0.968	± 0.746	± 0.969	± 1.190	± 1.454
0.229	0.296	0.371	0.485	0.031	-0.017	-0.076	-0.137
$\bar{0}.177$	$\bar{0}.293$	$\bar{0}.439$	$\bar{0}.665$	$\bar{0}.117$	$\bar{0}.169$	$\bar{0}.235$	$\bar{0}.373$
0.028	0.072	0.139	0.250	0.063	0.131	0.242	0.484
± 0.032	± 0.060	± 0.105	± 0.200	$\bar{0}.014$	$\bar{0}.054$	$\bar{0}.140$	$\bar{0}.356$
-0.023	-0.065	-0.146	-0.333	-0.006	0.001	0.031	0.122
± 0.002	± 0.016	± 0.051	± 0.143	± 0.007	± 0.019	± 0.037	± 0.097
0.006	0.018	0.045	0.125	-0.004	-0.017	-0.057	-0.219
$\bar{0}.004$	$\bar{0}.019$	$\bar{0}.064$	$\bar{0}.222$	0.000	± 0.008	± 0.042	± 0.217
0.000	0.004	0.023	0.100	0.001	0.000	-0.015	-0.117
± 0.001	± 0.006	± 0.022	± 0.091	$\bar{0}.001$	$\bar{0}.003$	$\bar{0}.007$	$\bar{0}.017$
-0.001	-0.006	-0.032	-0.167	0.000	0.003	0.017	0.122

2.1

FOR $\lambda = 0.25$



$x_p/c = 0.0$

$x_p/c = \pm 0.125$

$n \backslash \mu$	$x_p/c = 0.0$				$x_p/c = \pm 0.125$			
	0.90	0.94	0.97	1.00	0.90	0.94	0.97	1.00
0	1.484	1.605	1.698	1.792	1.480	1.604	1.699	1.795
1	0	0	0	0	± 0.335	± 0.386	± 0.427	± 0.469
2	0.554	0.691	0.817	0.965	0.479	0.598	0.709	0.842
3	0	0	0	0	∓ 0.194	∓ 0.274	∓ 0.354	∓ 0.455
4	-0.172	-0.262	-0.361	-0.498	-0.094	-0.139	-0.191	-0.264
5	0	0	0	0	± 0.096	± 0.166	± 0.251	± 0.380
6	0.068	0.128	0.206	0.333	0.007	0.009	0.012	0.018
7	0	0	0	0	∓ 0.042	∓ 0.089	∓ 0.157	∓ 0.280
8	-0.030	-0.070	-0.132	-0.250	0.010	0.028	0.055	0.109
9	0	0	0	0	± 0.016	± 0.040	± 0.081	± 0.169
10	0.014	0.041	0.090	0.200	-0.010	-0.031	-0.071	-0.163
11	0	0	0	0	∓ 0.004	∓ 0.012	∓ 0.027	∓ 0.064
12	-0.007	-0.025	-0.064	-0.167	0.006	0.023	0.061	0.166

TABLE

q_n COEFFICIENTS

$$x_p/c = \pm 0.25$$

$$x_p/c = \pm 0.375$$

$x_p/c = \pm 0.25$				$x_p/c = \pm 0.375$			
0.90	0.94	0.97	1.00	0.90	0.94	0.97	1.00
1.462	1.595	1.698	1.804	1.411	1.561	1.687	1.819
± 0.645	± 0.756	± 0.846	± 0.939	± 0.882	± 1.068	± 1.233	± 1.413
0.268	0.329	0.390	0.471	-0.018	-0.065	-0.109	-0.147
$\bar{0}.266$	$\bar{0}.380$	$\bar{0}.501$	$\bar{0}.662$	$\bar{0}.156$	$\bar{0}.206$	$\bar{0}.267$	$\bar{0}.371$
0.062	0.112	0.170	0.250	0.115	0.195	0.302	0.483
± 0.054	± 0.086	± 0.128	± 0.199	$\bar{0}.044$	$\bar{0}.102$	$\bar{0}.192$	$\bar{0}.356$
-0.055	-0.111	-0.191	-0.333	-0.001	0.017	0.052	0.122
± 0.012	± 0.035	± 0.073	± 0.143	± 0.016	± 0.029	± 0.048	± 0.097
0.015	0.033	0.062	0.125	-0.013	-0.038	-0.087	-0.219
$\bar{0}.015$	$\bar{0}.043$	$\bar{0}.097$	$\bar{0}.222$	± 0.005	± 0.024	± 0.072	± 0.217
0.003	0.013	0.038	0.100	0.000	-0.006	-0.031	-0.117
± 0.005	± 0.014	± 0.034	± 0.091	$\bar{0}.002$	$\bar{0}.006$	$\bar{0}.009$	$\bar{0}.017$
-0.004	-0.018	-0.055	-0.167	0.002	0.009	0.031	0.122

LE 2.2

TS FOR $\lambda = 0.375$

$$x_p/c = 0.0$$

$$x_p/c = \pm 0.125$$

n \ μ	$x_p/c = 0.0$				$x_p/c = \pm 0.125$			
	0.90	0.94	0.97	1.00	0.90	0.94	0.97	1.00
0	1.286	1.381	1.454	1.527	1.285	1.382	1.456	1.531
1	0	0	0	0	± 0.348	± 0.388	± 0.420	± 0.452
2	0.614	0.730	0.831	0.945	0.529	0.631	0.720	0.823
3	0	0	0	0	∓ 0.238	∓ 0.309	∓ 0.374	∓ 0.453
4	-0.222	-0.306	-0.389	-0.496	-0.118	-0.161	-0.205	-0.263
5	0	0	0	0	± 0.134	± 0.203	± 0.278	± 0.380
6	0.100	0.162	0.232	0.332	0.008	0.010	0.013	0.018
7	0	0	0	0	∓ 0.067	∓ 0.118	∓ 0.181	∓ 0.280
8	-0.051	-0.096	-0.154	-0.250	0.019	0.039	0.066	0.109
9	0	0	0	0	± 0.028	± 0.056	± 0.097	± 0.169
10	0.027	0.060	0.110	0.200	-0.020	-0.047	-0.088	-0.163
11	0	0	0	0	∓ 0.008	∓ 0.017	∓ 0.033	∓ 0.064
12	-0.015	-0.040	-0.081	-0.167	0.014	0.037	0.079	0.166

TABLE

a_n COEFFICIENTS

$$x_p/c = \pm 0.25$$

$$x_p/c = \pm 0.375$$

$x_p/c = \pm 0.25$				$x_p/c = \pm 0.375$			
0.90	0.94	0.97	1.00	0.90	0.94	0.97	1.00
1.277	1.382	1.463	1.545	1.244	1.366	1.465	1.568
± 0.677	± 0.766	± 0.835	± 0.906	± 0.944	± 1.100	± 1.230	± 1.367
0.287	0.341	0.393	0.456	-0.056	-0.097	-0.130	-0.157
$\bar{0}.328$	$\bar{0}.432$	$\bar{0}.533$	$\bar{0}.658$	$\bar{0}.181$	$\bar{0}.229$	$\bar{0}.284$	$\bar{0}.367$
0.091	0.139	0.188	0.250	0.158	0.241	0.338	0.483
± 0.071	± 0.104	± 0.142	± 0.199	$\bar{0}.074$	$\bar{0}.140$	$\bar{0}.224$	$\bar{0}.356$
-0.085	-0.145	-0.219	-0.333	0.007	0.031	0.066	0.122
± 0.024	± 0.051	± 0.086	± 0.143	± 0.023	± 0.037	± 0.056	± 0.097
0.024	0.044	0.073	0.125	-0.025	-0.057	-0.109	-0.219
$\bar{0}.028$	$\bar{0}.064$	$\bar{0}.119$	$\bar{0}.222$	± 0.014	± 0.042	± 0.095	± 0.217
0.008	0.023	0.049	0.100	-0.002	-0.015	-0.045	-0.117
± 0.009	± 0.022	± 0.044	± 0.091	$\bar{0}.004$	$\bar{0}.007$	$\bar{0}.010$	$\bar{0}.017$
-0.011	-0.032	-0.073	-0.167	0.005	0.017	0.043	0.122

LE 2.3

ITS FOR $\lambda = 0.50$

RES

$$x_p/c = 0.0$$

$$x_p/c = \pm 0.125$$

n \ μ	$x_p/c = 0.0$				$x_p/c = \pm 0.125$			
	0.90	0.94	0.97	1.00	0.90	0.94	0.97	1.00
0	1.130	1.209	1.269	1.330	1.131	1.212	1.273	1.336
1	0	0	0	0	± 0.347	± 0.381	± 0.407	± 0.433
2	0.645	0.745	0.829	0.923	0.555	0.643	0.719	0.802
3	0	0	0	0	∓ 0.268	∓ 0.330	∓ 0.386	∓ 0.449
4	-0.258	-0.334	-0.406	-0.494	-0.136	-0.176	-0.214	-0.261
5	0	0	0	0	± 0.164	± 0.230	± 0.295	± 0.379
6	0.127	0.186	0.248	0.332	0.009	0.011	0.014	0.018
7	0	0	0	0	∓ 0.088	∓ 0.140	∓ 0.197	∓ 0.279
8	-0.069	-0.116	-0.170	-0.249	0.027	0.048	0.073	0.109
9	0	0	0	0	± 0.039	± 0.070	± 0.108	± 0.169
10	0.040	0.076	0.123	0.200	-0.031	-0.060	-0.099	-0.163
11	0	0	0	0	∓ 0.012	∓ 0.022	∓ 0.038	∓ 0.064
12	-0.025	-0.053	-0.094	-0.166	0.023	0.050	0.091	0.166

TABLE 2
 q_n COEFFICIENTS I

$$x_p/c = \pm 0.25$$

$$x_p/c = \pm 0.375$$

$x_p/c = \pm 0.25$				$x_p/c = \pm 0.375$			
0.90	0.94	0.97	1.00	0.90	0.94	0.97	1.00
1.132	1.219	1.286	1.354	1.114	1.218	1.300	1.384
± 0.683	± 0.756	± 0.813	± 0.871	± 0.966	± 1.099	± 1.207	± 1.319
0.295	0.344	0.388	0.440	-0.086	-0.120	-0.146	-0.167
$\bar{0}.371$	$\bar{0}.465$	$\bar{0}.551$	$\bar{0}.653$	$\bar{0}.197$	$\bar{0}.244$	$\bar{0}.293$	$\bar{0}.363$
0.112	0.157	0.199	0.250	0.193	0.274	0.361	0.482
± 0.085	± 0.117	± 0.151	± 0.198	$\bar{0}.102$	$\bar{0}.169$	$\bar{0}.246$	$\bar{0}.356$
-0.110	-0.171	-0.238	-0.332	0.017	0.043	0.076	0.123
± 0.035	± 0.063	± 0.096	± 0.143	± 0.029	± 0.043	± 0.062	± 0.097
0.032	0.054	0.081	0.125	-0.038	-0.073	-0.124	-0.219
$\bar{0}.043$	$\bar{0}.082$	$\bar{0}.135$	$\bar{0}.222$	± 0.024	± 0.058	± 0.112	± 0.217
0.013	0.031	0.057	0.100	-0.006	-0.024	-0.055	-0.117
± 0.014	± 0.029	± 0.050	± 0.091	$\bar{0}.006$	$\bar{0}.008$	$\bar{0}.010$	$\bar{0}.017$
-0.018	-0.044	-0.086	-0.167	0.009	0.024	0.053	0.122

E 2.4

S FOR $\lambda = 0.625$

$$x_p/c = \pm 0.25$$

$$x_p/c = \pm 0.375$$

$x_p/c = \pm 0.25$				$x_p/c = \pm 0.375$			
0.90	0.94	0.97	1.00	0.90	0.94	0.97	1.00
1.015	1.090	1.147	1.205	1.011	1.101	1.171	1.242
± 0.673	± 0.737	± 0.786	± 0.835	± 0.967	± 1.083	± 1.175	± 1.270
0.297	0.341	0.380	0.424	-0.109	-0.138	-0.158	-0.175
$\bar{0}.401$	$\bar{0}.485$	$\bar{0}.560$	$\bar{0}.647$	$\bar{0}.209$	$\bar{0}.253$	$\bar{0}.298$	$\bar{0}.358$
0.129	0.170	0.207	0.250	0.222	0.299	0.377	0.480
± 0.096	± 0.126	± 0.157	± 0.197	$\bar{0}.126$	$\bar{0}.191$	$\bar{0}.261$	$\bar{0}.356$
-0.132	-0.190	-0.251	-0.332	0.026	0.053	0.083	0.123
± 0.045	± 0.073	± 0.102	± 0.143	± 0.034	± 0.048	± 0.066	± 0.097
0.040	0.061	0.087	0.125	-0.049	-0.087	-0.136	-0.219
$\bar{0}.056$	$\bar{0}.097$	$\bar{0}.146$	$\bar{0}.222$	± 0.035	± 0.072	± 0.125	± 0.217
0.019	0.038	0.062	0.100	-0.011	-0.031	-0.062	-0.117
± 0.019	± 0.034	± 0.055	± 0.091	$\bar{0}.007$	$\bar{0}.009$	$\bar{0}.011$	$\bar{0}.017$
-0.026	-0.055	-0.096	-0.166	0.014	0.031	0.060	0.122

LE 2.5

TS FOR $\lambda = 0.75$

0.7845	0.3927	0	-0.0005	0	0.0000	0
-0.2544	0	-0.1273	0	0.0001	0	0.0000
0.0018	0.0637	0	-0.0628	0	0.0000	0
0.0003	0	0.0419	0	-0.0417	0	0.0000
0.0000	0.0000	0	0.0313	0	-0.0313	0
0.0000	0	0.0000	0	0.0250	0	-0.0250
0.0000	0.0000	0	0.0000	0	0.0208	0

TABLE 3.1
[s] MATRIX FOR $\lambda = 0.25$

1.2088	0.6058	0	-0.0014	0	0.0000	0
-0.5177	0	-0.2599	0	0.0011	0	0.0000
0.0057	0.1300	0	-0.1274	0	0.0003	0
0.0021	0	0.0849	0	-0.0840	0	0.0001
0.0000	-0.0003	0	0.0630	0	-0.0628	0
0.0000	0	-0.0001	0	0.0502	0	-0.0501
0.0000	0.0000	0	-0.0001	0	0.0418	0

TABLE 3.2

[s] MATRIX FOR $\lambda = 0.50$

1.4971	0.7496	0	-0.0009	0	-0.0001	0
-0.7777	0	-0.3919	0	0.0031	0	0.0000
0.0040	0.1959	0	-0.1950	0	0.0010	0
0.0061	0	0.1300	0	-0.1273	0	0.0004
0.0005	-0.0008	0	0.0955	0	-0.0947	0
0.0000	0	-0.0004	0	0.0757	0	-0.0755
0.0000	0.0000	0	-0.0002	0	0.0629	0

TABLE 3.3

[S] MATRIX FOR $\lambda = 0.75$

Approved Distribution List for

The Ducted Propeller In Static And Low-Speed Flight

issued under Contract Nonr-4357(00), Office of Naval Research

Chief, Bureau of Naval Weapons
(RAAD-3)
Department of the Navy
Washington, D. C. 20360

Chief, Bureau of Naval Weapons
(RAAD-22)
Department of the Navy
Washington, D. C. 20360

Chief, Bureau of Naval Weapons
(RAAD-32)
Department of the Navy
Washington, D. C. 20360

Chief, Bureau of Naval Weapons
(RAAD-33)
Department of the Navy
Washington, D. C. 20360

Chief, Bureau of Naval Weapons
(RA-4)
Department of the Navy
Washington, D. C. 20360

Chief, Bureau of Naval Weapons
(R-55)
Department of the Navy
Washington, D. C. 20360

Chief, Bureau of Naval Weapons
(RRRE-4)
Department of the Navy
Washington, D. C. 20360

Commanding Officer
U. S. Army Transportation Research
Command
Fort Eustis, Virginia
ATTN: Aero Mechanics Group (1 copy)

Chief of Naval Research
(Code 461)
Department of the Navy
Washington, D. C. 20360 (6 copies)

Chief of Naval Research
(Code 438)
Department of the Navy
Washington, D. C. 20360

Commanding Officer
Office of Naval Research Branch
Office
Navy #100, Box 39, F.P.O.
New York, New York (1 copy)
ATTN: CDR Donald Farsching

Commanding Officer
Officer of Naval Research Branch
Office
346 Broadway
New York 13, New York

Director
Naval Research Laboratory
Technical Information Office
Washington, D. C. 20390 (1 copy)

Commander
Army Material Command
ATTN: AMCRD-RS-PE-A
Department of the Army
Washington, D. C. 20315

Commanding Officer and Director
David Taylor Model Basin
Aerodynamics Laboratory Library
Washington, D. C. 20007

Army Research Office
Physical Sciences Division
ATTN: Mr. R. Ballard
3045 Columbia Pike
Arlington, Virginia 20310

U. S. Air Force (SRGL)
Office of Scientific Research
Washington 25, D. C.

Commanding Officer and Director
David Taylor Model Basin
Aerodynamics Laboratory
Washington, D. C. 20007
ATTN: Mr. H. Chaplin

Mr. Maurice Sevik
Ordnance Research Laboratory
Pennsylvania State University
P. O. Box 30
University Park, Pennsylvania

Mr. Paul Granville
Hydrodynamics Laboratory
David Taylor Model Basin
Code 581
Washington, D. C. 20007

Commanding Officer and Director
David Taylor Model Basin
Hydrodynamics Laboratory
Washington, D. C. 20007
ATTN: Dr. William B. Morgan

Pennsylvania State University
Aeronautical Engineering Department
University Park, Pennsylvania
ATTN: Dr. B. W. McCormick

Grumman Aircraft Engineering Corp.
Bethpage, Long Island, New York
ATTN: Mr. F. T. Kurt

Ryan Aeronautical Company
Lindbergh Field
San Diego, California
ATTN: Mr. H. James

United Aircraft Corporation
Hamilton Standard Division
Windsor Locks, Connecticut
ATTN: Mr. G. Rosen

Bureau of Ships
Department of the Navy
Washington 25, D. C.
ATTN: Mr. David Berg, Code 436

Mr. W. D. Crater
Management Technology Inc.
8939 South Sepulveda Boulevard
Los Angeles 45, California

Mr. V. O. Hoehne
Battelle Memorial Institute
505 King Avenue
Columbus 1, Ohio

Vertol Division
Boeing Airplane Company
Woodland Avenue
Morton, Pennsylvania
ATTN: Mr. W. Z. Stepniewski

Massachusetts Institute of
Technology
Aeronautical Engineering Dept.
Cambridge 30, Mass.
ATTN: Prof. R. H. Miller

Mr. H. V. Borst
Chief Engineer, Technical Services
VTOL Systems Group
Curtiss-Wright Corporation
Caldwell, New Jersey

McDonnell Aircraft Corporation
St. Louis, Missouri
ATTN: Dr. Kurt Hohenemser

Mr. J. E. Nichols, Manager
Advanced Planning & Research
Division
Hiller Aircraft Company
Palo Alto, California

Davidson Laboratory
Stevens Institute of Technology
Hoboken, New Jersey
ATTN: Dr. J. P. Breslin

Graduate School of Aerospace
Engineering
290 Grumman Hall
Cornell University
Ithaca, New York
ATTN: Prof. E. L. Resler

Department of Aeronautical
Engineering
Princeton University
Princeton, New Jersey
ATTN: Prof. D. Hazen

Research and Technology Division
ATTN: SESSC (Mr. Lindenbaum)
Wright-Patterson AFB, Ohio 45433

Defense Documentation Center
Hq., Cameron Station
Building #5
Alexandria, Virginia 22314
(20 copies)

National Aeronautics and Space
Administration
600 Independence Avenue, S. W.
ATTN: Code RA, Code RAD
Washington, D. C. 20546 (2 copies)

National Aeronautics and Space
Administration
Langley Research Center
Langley Research Station
Hampton, Virginia 23365
ATTN: Mr. P. Donely

National Aeronautics and Space
Administration
Ames Research Center
Moffat Field, California
ATTN: Mr. W. Cook

Air Warfare Research Division
Naval Air Development Center
Johnsville, Pennsylvania
ATTN: Mr. Jack Triem

Capt. W. C. Bergstedt
Commanding Officer
Scientific and Technical Unit
CINCUSNAVEUR Representative
Frankfort, Germany
APO 757, New York, New York

Library
American Institute of Aeronautics
and Astronautics
750 Third Avenue
New York 17, New York (1 copy)

Cornell Aeronautical Lab., Inc.
4455 Genesee Street
Buffalo 21, New York
ATTN: Technical Director
Mr. H. A. Cheilek

Collins Radio Company
Cedar Rapids, Iowa
ATTN: Dr. A. Lippisch

Mr. A. M. O. Smith, Supervisor
Aerodynamics Research Group
Aircraft Division
Douglas Aircraft Co., Inc.
Long Beach, California

Electric Boat Division
General Dynamics Corporation
Groton, Connecticut
ATTN: GEM Section
Research and Development
Annex
Mr. E. Davison

Georgia Institute of Technology
School of Aerospace Engineering
Atlanta, Georgia 30332
ATTN: Prof. D. W. Dutton

Vehicle Research Corporation
1661 Lombardy Road
Pasadena, California
ATTN: Dr. Scott Rethorst

University of Virginia
Aerospace Engineering Department
Charlottesville, Virginia
ATTN: Dr. G. B. Matthews

Mississippi State University
Engineering and Industrial
Research Station
State College, Mississippi
ATTN: Dr. J. J. Cornish

Vidya Division
1450 Page Mill Road
Stanford Industrial Park
Palo Alto, California
ATTN: Dr. J. N. Nielsen

Naval Postgraduate School
Aeronautical Engineering
Department
Monterey, California
ATTN: Dr. R. Head

General Electric Company
Flight Propulsion Division
Cincinnati 15, Ohio
ATTN: Mr. R. Goldsmith

Mr. Robert Postle
Bell Aerosystems Company
Buffalo 5, New York

Republic Aviation Corporation
Farmingdale, Long Island
New York
ATTN: Mr. J. Maravel